# Three-Dimensional Printing of Acrylonitrile Butadiene Styrene Microreactors for Photocatalytic Applications

*Aarón Cabrera,[†] Ismael Pellejero,[*,†], Tamara Oroz-Mateo,[‡] Cristina Salazar,[‡] Alberto Navajas,[†] Claudio Fernández-Acevedo,[‡] Luis M. Gandía[†]*

† Institute for Advanced Materials and Mathematics (InaMat$^2$), Universidad Pública de Navarra (UPNA), Edificio Jerónimo de Ayanz, Campus de Arrosadia, Pamplona, Navarra, 31006 Spain.

‡ Centro Tecnológico Lurederra, Industrial Area Perguita, C/A Nº 1, Los Arcos, Navarra, 31210 Spain.

**KEYWORDS.** Microreactor; ABS polymer; 3D printing; Photocatalysis; Cu-$TiO_2$ Nanoparticles; Flame Spray Pyrolysis.

**ABSTRACT.** Miniaturization is a key aspect for many technological applications and the use of microreactors is an excellent solution for the intensification of chemical processes for a variety of applications. However, standard microfabrication requires large facilities and intricate fabrication protocols, and consequently it is not easily available, generally resulting in high production costs. Herein, we present a very cheap, fast and easy microreactor design for photocatalytic applications based on direct fused filament 3D printing as a facilitating and

widespread technology. The microreactor consists of three bodies directly printed in ABS (Acrylonitrile Butadiene Styrene): a main body with a serpentine microchannel pattern where the photocatalyst is placed, a top holder with a transparent polymer window, and a base to clamp the parts. Several microreactor units were coated with $TiO_2$ doped with Cu (2.4 wt.%) nanoparticles synthesized by FSP (Flame Spray Pyrolysis) and tested for the photocatalytic degradation of two water pollutants showing excellent performance.

## INTRODUCTION

Green chemistry is a route toward production sustainability, and microreactors are one of the tools available to make it possible, thanks to their enhanced mass and heat transport properties in comparison to conventional reactors.[1–3] A microreactor is a device with interconnected microchannels in which a chemical reaction is carried out. The inner characteristic dimensions are typically below 1 mm. This miniaturization mainly offers high surface-to-volume ratio, controllable interaction between reactants and mass diffusion, lower energy consumption, excellent heat exchange and temperature control, minimization of light loss in photoreactions, better product selectivity, and the opportunity to integrate processes in an automated manner.[4–6] These features make microreactors an ideal solution to handle multiple reaction systems,[7–10] especially in heterogeneous photocatalysis, where a close interaction between the incident light, catalyst and reactants is much needed and hardly achieved in conventional systems.[11,12]

Microreactors, like other microfluidic devices, can be manufactured by different techniques such as standard photolithography, soft lithography, micromolding or laser ablation, and a large variety of construction materials are available, such as silicon, glass, polymers, and metals.[13,14] Mainly, polydimethylsiloxane (PDMS) elastomer has been used as construction material due to its outstanding properties of biocompatibility, flexibility, and optical transparency in the UV-Vis

range, which make it appropriate for multiple applications, including photocatalysis and photochemistry.[15,16] PDMS microchannel reactors have been fabricated by soft lithography followed by casting and bonding processes.

Nowadays, direct 3D printing (additive manufacturing) of microdevices is attracting more and more attention due to its versatility, low cost, simplicity, availability, and rapid prototyping.[17,18] Among the different types of 3D-printing techniques,[19] fused filament fabrication (FFF) (also known as Fused Deposition Modeling – FDM) has become the most popular because of its suitability even for homemade applications and its very low cost. FFF allows 3D objects to be created through layer-by-layer addition of a fused polymer filament under precise digital control. The resolution depends on the diameter of the nozzle through which the thermoplastic is extruded (0.2–0.8 mm), and satisfactory values are achieved for many applications. The ease of use, fast prototyping and roughly micro-scale accuracy make FFF 3D-printing an ideal tool for fast manufacture of microfluidic devices in different fields of application.[20–23]

Photocatalysis is one of the areas where microreactor prototyping by 3D printing can have a big impact. Figure 1 depicts the three fabrication protocols assisted by 3D FFF that can be followed to manufacture photocatalytic microreactors:

i) The molding and PDMS replica protocol is based on the standard fabrication of microfluidic devices. In this case, the mold is directly built by 3D printing instead of regular SU-8 photopolymer fabrication by photolithography techniques in sophisticated clean-room facilities.[24,25] The advantages are the ability to reuse the mold can be reused, the ease of incorporation of the photocatalyst directly on the channels, and much better scale-out possibilities of the microreactors because they can be mounted in three dimensions due to their

complete transparency.[26,27] In contrast, a plasma bonding is necessary to seal the union with another PDMS or glass piece, which makes the process difficult.

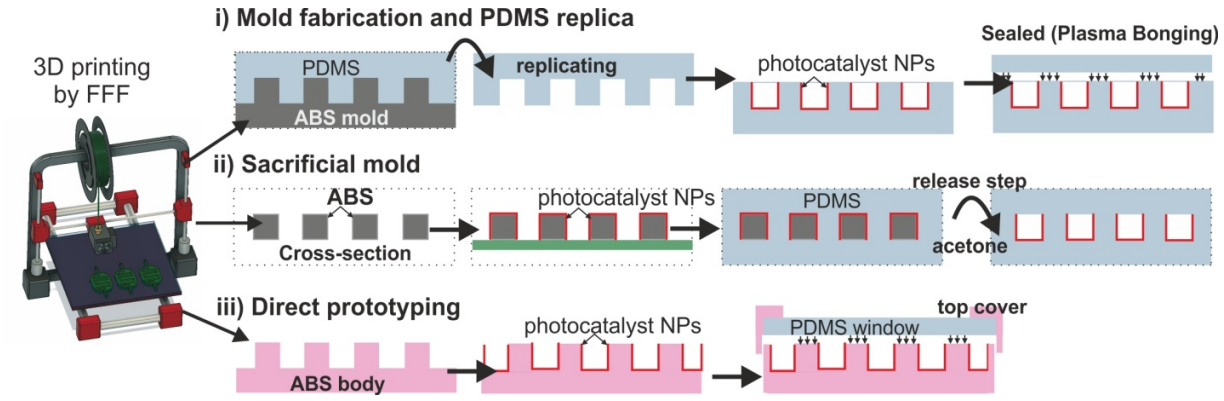


**Figure 1.** Fabrication protocols of photocatalytic microchannel reactors assisted by FFF 3D printing: i) mold and replica, ii) sacrificial mold and iii) direct prototyping proposed in this work.

ii) The sacrificial mold protocol follows the idea proposed by Saggiomo and Velders,[28,29] where negative channels are directly 3D printed in ABS and subsequently immersed into PDMS, and then the ABS is dissolved in acetone, releasing the channels. Here, the distinguishing advantages are that the whole of the PDMS block is one piece, avoiding any leakage, allowing intricate and multilevel microchannel designs to be carry out, and offering full integration of the photocatalyst in the reactor walls; however, the release step of the sacrificial ABS mold can be very tedious for channels with a of characteristic dimension below 1 mm;[30] in addition, the mold is lost and waste is generated.

iii) Direct prototyping of the microreactor by an FFF-type printer allows versatile, fast, and easy fabrication of microfluidic devices,[17,18,31] but unfortunately, there are no whole range transparent (UV-Vis) materials that permit light to pass through them to be accessible to the photocatalyst. To solve this, in this work, a three-part reactor design is proposed, including a PDMS cover to seal the channels and serve as an optical window. In addition to the easy

fabrication of the microreactor body, the photocatalyst can be straightforwardly integrated on the channels by, for example,. drop-coating; however, as the main body of the microreactor is opaque, only scaling-out in the same plane is allowed.

Here, we have implemented reactor dimensions for correct and accurate 3D printing, made different modifications of the wall design and studied the effects of the PDMS curing parameters to achieve good sealing and prevent leaking and bypassing. The reactor could also be directly printed on a composite filament (ABS + photocatalyst)[32–34] with only slight changes in the printing parameters, further simplifying the fabrication. This cheap and fast procedure could facilitate the use of microreactors in photocatalyst testing and increase the possibilities of process intensification with microchannel reactors.

## MATERIALS AND METHODS

### *Photocatalyst Nanoparticles Production*

The synthesis of $TiO_2$ nanoparticles (NPs) doped with Cu (Cu-$TiO_2$) was carried out by the Flame Spray Pyrolysis (FSP)[35,36] technique. Preliminary studies carried out in our laboratories with different Cu loadings (see Graph 1 in Figure S1 of the Supplementary Information – SI) showed that 2.4 wt.% Cu presented a superior catalytic performance. So, an FSP pilot plant constructed by Lurederra Technology Centre with a production capacity of 100 g $h^{-1}$ was primarily optimized to adjust the flame parameters for the target material composition (2.4 wt.% Cu on $TiO_2$ and bare $TiO_2$ for comparative experiments). This one-step process begins with the controlled feeding of a liquid mixture of the metallic precursors through an atomizer into a high-temperature flame (see Images A and B of Figure S1 of the SI). This mixture was based on ethylhexanoate, propoxide and acetylacetonate of Ti and Cu in an atomic ratio of 1:32 (Cu:Ti),

combined with isopropyl alcohol and acetic acid as solvents and suitable additives to adjust the heat of combustion and viscosity. The precursor flow rates studied were in the range of 10–30 mL·min$^{-1}$. The dispersion gas ($O_2$) was set at 30–40 mL·min$^{-1}$, and the nozzle pressure was typically around 2-4 bar. Cu-$TiO_2$ nanoparticles were collected downstream by a specific sleeve filter system. Physicochemical characterization was carried out by several techniques: XRD (D-Max Rigaku, Ru300), diffuse reflectance (Flame Ocean Optics spectrophotometer with reflectance probe), $N_2$ adsorption (Tristar II 3020 multi-sample specific surface area analyzer) and TEM-EDS (FEI Tecnai F30 transmission electron microscope).

***Microreactor Design and Fabrication***

The design of the microreactors was performed with computer-aided design software (SolidWorks®). As depicted in Figure 2, the ensemble consists of three parts: a main body containing a serpentine-shape channel with a trapezoidal section (1.5 × 1 × 0.5 mm) and channel volume of *ca*. 0.3 mL, a top cover with a transparent PDMS (polydimethylsiloxane) window, and a base, with the complete device being held by four 3D printed clamps. ABS polymer was selected as the construction material because of its good thermal and mechanical properties coupled with easy extrusion.[37] The printing parameters were adjusted by the slicing application Ultimaker Cura® and the three parts were printed in ABS (SMARTFIL® ABS Smart Materials 3D) using an affordable 3D printer Creality Ender 3 (extrusion parameters: nozzle 400 µm, 235 ºC, 1.75 mm filament). STL files, detailed drawings, and additional details about Cura slicing parameters are available in the SI (Table S1).

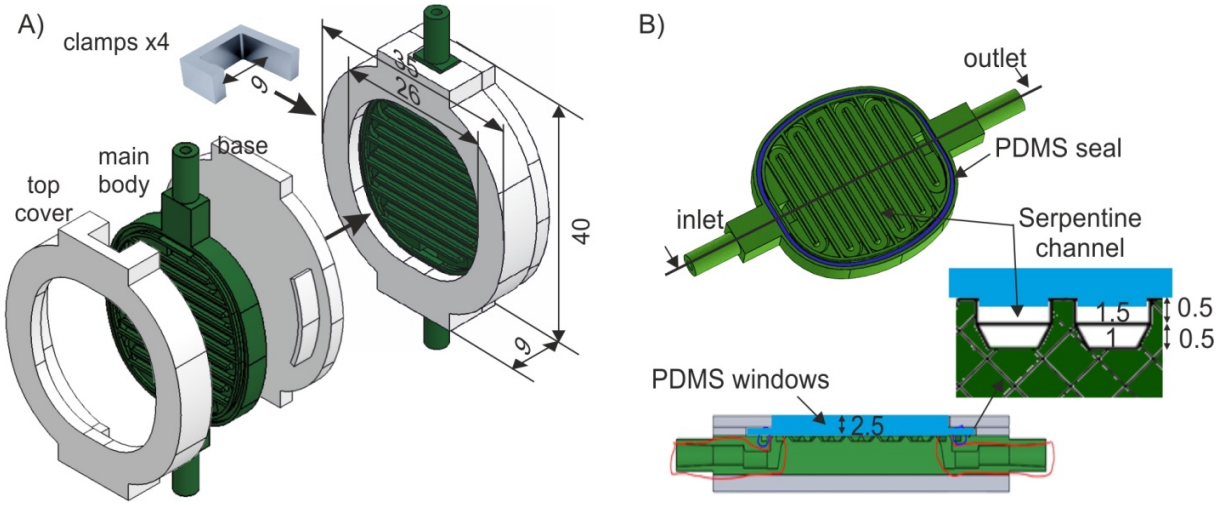


**Figure 2.** A) Assembly scheme of the microreactor parts including clamps for holding the group together and B) main body, top view and cross-section of the serpentine channel (dimensions in mm).

Prior to assembling and sealing the parts together, the main body was coated with 3 mg of the Cu-$TiO_2$ photocatalyst by the drop-coating method. To this end, 10 mg of Cu-$TiO_2$ NPs were dispersed in 1 mL of $H_2O$ 1:1 propane-1,2-diol (Aldrich) (v/v), the dissolution was sonicated vigorously, and afterwards 100 µL of the dispersion was deposited homogeneously with a micropipette on the serpentine channel. Drying was conducted in an oven at 100 °C for 15 min. The process was repeated three times to attain 3 mg of coating, which corresponds to a catalyst loading of *ca*. 0.85 mg·$cm^{-2}$.

The different steps followed for assembling the microreactor components are represented in the scheme of Figure S2 in the SI. In brief: (i) the optical window in the top cover part was fabricated from a UV-VIS transparent (from 300 to 800 nm) polymer PDMS (Sylgard 184, Dow Chemical Company), mixing the prepolymer (elastomer) and the curing agent (cross-linker) in a 10:0.8 (w/w) ratio and degassed under vacuum (20 mm Hg) for 30 min; (ii) then, the top cover

piece was stuck face-up on scotch tape and *ca*. 1.4 g of liquid PDMS was poured on the hole for the window; (iii) then, the piece was placed in an oven for 9 min at 70 °C, after which the PDMS was half cured and remained slightly liquid; (iv) finally, the main body and the base were carefully located face-down on the cover to seal the reactor and the group was clamped with the PDMS. The assembled parts were kept in the oven for 15 min to harden the PDMS. The resulting thickness of the final PDMS window was *ca*. 2.5 mm.

***Photocatalytic experiments***

Two different photocatalytic reactions were selected to study the catalytic behaviour of the Cu-$TiO_2$ NPs and the microreactor performance: the photooxidation of 10 $mg \cdot L^{-1}$ of methylene blue (MB) (Panreac) and the photoreduction of 20 $mg \cdot L^{-1}$ of 4-nitrophenol (4NP) (Aldrich) in water using 1 $mg \cdot mL^{-1}$ of $NaBH_4$ (Aldrich) as reducing agent. Blank reactions were also performed with microreactors coated with undoped $TiO_2$ NPs. Photoreactions were carried out using the experimental set-up shown in Figure S3 of the SI. Briefly, a highly efficient 2 W LED at 365 ± 2 nm (1200 mW radiant flux) (Engin LZ1-10U600) was selected as the source of light. The reactor was placed under de LED at a distance of 25 mm. Reaction monitoring was performed by UV-Vis spectrometry following the absorbance peak decay at 400 nm for 4NP photoreduction to 4-aminophenol (4AP), and the absorbance lines at 663 nm (monomer) and 615 nm (dimer) for MB photodegradation.[38,39] Absorption spectra were collected every minute by using a compact spectrophotometer (Flame, Ocean Optics) with a very low volume flow cell that was placed downstream (dead volume *ca.* 80 µL). Experiments were carried out at different liquid flow rates from 2.5 to 20 $mL \cdot h^{-1}$ corresponding to residence times ($t_r$) of 432 to 54 s, respectively.

## RESULTS AND DISCUSSION

### *Photocatalyst characterization*

FSP has been demonstrated to be a versatile technique for the controlled production of oxides doped with other co-catalyst elements for photocatalytic applications.[40–42] Homogeneity and excellent chemical compatibility are required for the precursor liquid mixture, so it was prepared taking into account several aspects of chemical interactions such as solubility and viscosity of the compounds containing the metal cations (Ti and Cu). Several precursors such as ethylhexanoates, propoxides, acetylacetonates, acrylates, nitrates, butoxides, and acetates, solvents (ethanol, toluene, acetic acid, xylene, isopropanol, acetonitrile) and additives for viscosity control were considered. The selected final mixture resulted in a solution with a high heat of combustion of 30877 $kJ \cdot kg^{-1}$ to prevent incomplete combustion and a viscosity of 7 cps to facilitate the spray atomization through the nozzle during operation.

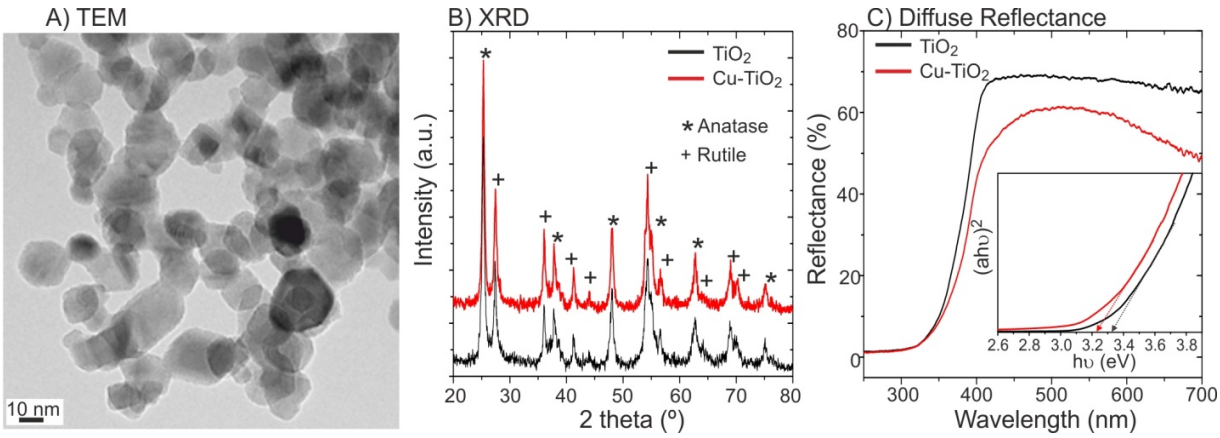


**Figure 3.** A) Representative TEM image, B) XRD pattern, and C) diffuse reflectance spectrum of Cu-$TiO_2$ NPs. Bare $TiO_2$ NPs data are included for comparison.

A representative TEM image of the FSP-synthesized Cu-$TiO_2$ NPs is shown in Figure 3A. During the FSP reaction, several processes occurred within a very short residence time (within the order of microseconds) in the flame, such as fine atomization, aerosol droplet evaporation, precursor combustion and oxide formation, agglomeration, sintering and surface growth. The process parameters, the mainly precursor feed rate, dispersion gas flow rate, and spray conditions including pressure, and so on were adjusted and optimized to achieve high purity, low aggregation and small particle size. The resulting particle mean diameter $d_p$ was $17.3 \pm 4.1$ nm and the BET specific area calculated from the $N_2$ adsorption experiments was 82.2 $m^2 \cdot g^{-1}$. EDS quantitative analysis indicated that the Cu content in the $TiO_2$ matrix was $1.62 \pm 0.25$ wt.%, and therefore, lower than the theoretical one in the precursor mixture (2.4 wt%). This result suggests that some part of the Cu was segregated during FSP synthesis, probably as CuO aggregates not incorporated in the $TiO_2$ matrix. XRD analyses (Figure 3B) show a similar ratio of anatase/rutile $TiO_2$ phases in both samples, with and without Cu (*ca*. 61% and 39% rutile).[43] The diffuse reflectance measurements (Figure 4C) show an absorption band in the visible region starting at *ca*. 550 nm for the Cu-containing sample, which is mainly due to the d-d transition of Cu(II) in the environment of crystalline of $TiO_2$.[44,45] From the Tauc plot (Figure 3C inset) the bandgap of the Cu-$TiO_2$ sample (3.21 eV) was barely red-shifted in comparison to bare $TiO_2$ (3.32 eV),[46] so we can assume that Cu is intercalated in the $TiO_2$ matrix.

***Microreactor fabrication***

The final printed main bodies and microreactors are shown in Figure 4. Inlet and outlet ducts are directly printed in the main body, facilitating connectivity to flexible tubing during operation. Achieving a perfect seal to avoid any leakage or bypassing between channels is essential for any

microfluidic device, so two modifications of the basic serpentine design were adopted: a perimeter-sealing channel in the main body piece and elevation of the channel walls. Sealing is performed with the PDMS of the optical window during the curing step. When assembling the serpentine channel with the top cover, part of the uncured PDMS must spill over the channel to seal the union, avoiding bypassing.

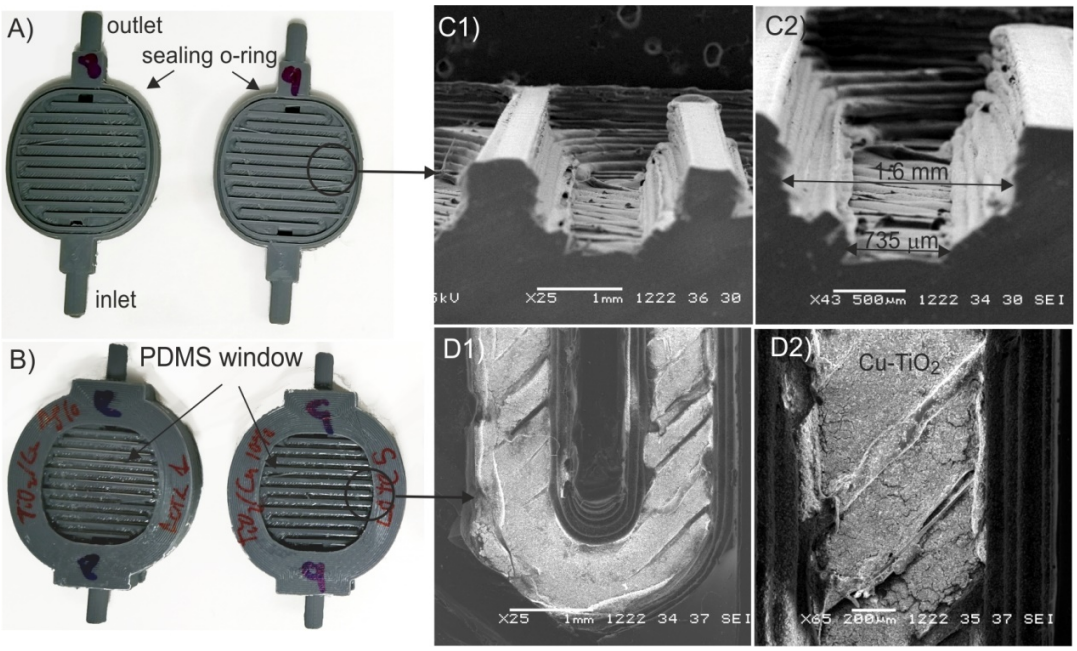


**Figure 4.** Photographs of 3D printed devices: A) main bodies and B) assembled microreactors SEM images of the serpentine channel: C) cross-section with trapezoidal shape prior to photocatalyst NP coating and D) top view of a channel coated with the catalyst.

The cross-section scheme depicted in Figure 2B illustrates how part of the channel is filled with the PDMS. Similarly, the perimeter-sealing channel over which excess the PDMS spills during assembly making a PDMS seal, is also marked. Another key parameter to achieve good sealing is the curing grade of the polymer prior to assembly; if the PDMS is slightly cured, channels can be blocked, but if it is completely cured it does not provide any sealing. So, after

several checks it was found that 9 min at 70 °C was the most favourable condition. Several microreactors were printed (Figure 4A) and assembled (Figure 4B) following the described procedures. All the printed microreactors were tested with 60 $mL \cdot h^{-1}$ of distilled water to corroborate that no leaks occurred under photocatalytic reaction conditions.

The SEM images in Figure 4C and 4D show the cross-section of the as-printed main body, indicating the final channel dimensions and the top view of the channel homogenously coated with the photocatalyst. The resolution of the printing can be improved by changing the 0.4 mm nozzle for a smaller one, that is, a 0.2-mm nozzle. Using a 0.2-mm nozzle, a microreactor with a squared 0.5 × 0.5 mm section was satisfactorily fabricated (see Figure S4); however, the increase in the printing time required, which reduced the production capacity, led us to select a larger section channel. Although the microreactor design was optimized to be fabricated by an FFF printer, in the case of needing much higher accuracy and precision in the channel dimensions, this same protocol can be followed by using SLA 3D printing with a proper photopolymer resin (see Figure S5); moreover, thanks to the new microSLA printers, this technology is affordable today.

***Photocatalytic reactor performance***

Several microreactors coated with Cu-$TiO_2$ NPs synthesized by FSP were employed for the degradation of two water pollutants; MB and 4NP. Photocatalytic experiments have demonstrated a much higher activity of Cu-$TiO_2$ NPs than bare $TiO_2$ (Figure 5). It is well known that the photoreduction of 4NP to 4AP is assisted by the electrons involved in the interaction of the semiconductor photocatalyst with light, while degradation of MB takes place by photooxidation of the organic matter by means of the photogenerated oxidant radicals ($OH^-$). At

a very low flow rate of 2.5 mL·h$^{-1}$ ($t_r$ = 432 s), the extent of the photoreduction of 4NP to 4AP (Figure 5A) reached a value above 99%, whereas for bare $TiO_2$ it was only 25%.

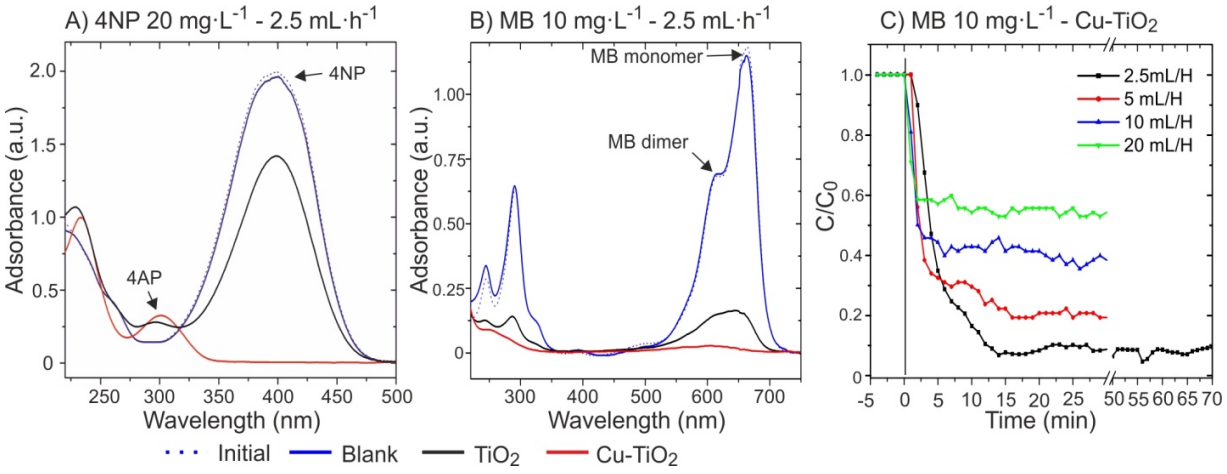


**Figure 5.** Photocatalytic experiments in the microreactors loaded with Cu-$TiO_2$ NPs at a feed flow rate of 2.5 mL·h$^{-1}$ ($t_r$ = 432 s) (spectra taken at a reaction time of 30 min): A) photoreduction of 20 mg·L$^{-1}$ 4NP to 4AP, and B) photodegradation of 10 mg·L$^{-1}$ MB. C) Monitoring of the degradation of 10 mg·L$^{-1}$ MB (wavelength 615 nm) at different feed flow rates (2.5, 5, 10, and 20 mL·h$^{-1}$).

As expected, the photoreduction of 4NP (Figure 5A) was efficiently catalyzed in the presence of metallic dopants like Cu.[47] At the same $t_r$, (Figure 5B) the MB photooxidation was practically completed (95% conversion) with Cu-$TiO_2$ NPs, while the conversion was also high (above 80%) for bare $TiO_2$, also evidencing a positive effect of the dopant on the photodegradation activity of titania.[48–50] Finally, Figure 5C shows the performance of the reactors at different flow rates corresponding to residence times from 54 to 432 s. As shown, once the UV LED is on, the MB absorbance (MB dimmer: λ = 615 nm) goes down, reaching a fluctuating value after approximately 15 min. At the highest feed flow rate employed, 20 mL·h$^{-1}$, which corresponds to a residence time below 1 min, *ca*. 40% conversion is achieved. This value increases up to 80%

for a residence time of about 3.5 min (5 $mL \cdot h^{-1}$), evidencing the good performance of the microchannels reactor, meaning that an efficient contact between light, the catalyst and the reactants is achieved.

It is also important to highlight the relevance of performing photocatalytic studies in microreactors in order to standardize results, compare materials, minimize reactant waste, screen photocatalysts, and study various reactor–catalyst configurations.[51]

## CONCLUSIONS

We have presented a new method of the fabrication of microchannel photoreactors where the pieces are directly 3D printed in ABS, avoiding casting and molding steps. By using this cheap and widely accessible technology (a fused filament printer), the fabrication of a variety of designs is possible without the need for access to microfabrication facilities. The fabricated microreactors have been employed in model reactions of photocatalytic applications. Sealing the microreactor parts to avoid any leakage was the key step of the procedure. This was accomplished during curing of the PDMS that forms the optical window. With good control of the curing time (9 min) and temperature (70 °C), microreactors could be sealed with the liquid PDMS without collapsing the microchannels as the same time as the transparent window was completed. Several microreactors were fabricated with Cu-$TiO_2$ NPs synthesized by FSP as photocatalytic coating for the photooxidation of methylene blue and the photoreduction of 4-nitrophenol. Photoactivity experiments have demonstrated the good performance of the microreactors at different residence times. It can be concluded that this cheap, easy, fast and widely available technique to fabricate microreactors could be very helpful to many researchers

to move into the world of microreaction and process intensification as well as to facilitate catalyst-screening studies.

## ASSOCIATED CONTENT

### Supporting Information

The following files are available free of charge.

Supplementary Figures and Information about 3D printing files and drawing (file type .PDF)

## AUTHOR INFORMATION

### Corresponding Author

* Ismael Pellejero

E-mail. Ismael.Pellejero@unavarra.es

Telephone: +34948166309

### Author Contributions

The manuscript was written with contributions by all authors. All authors have given approval to the final version of the manuscript.

### ORCID

Aarón Cabrera: 0000-0002-1860-9864

Ismael Pellejero: 0000-0002-8448-7543

Tamara Oroz-Mateo: 0000-0003-3407-8140

Cristina Salazar: 0000-0003-1936-1538

Claudio Fernández-Acevedo: 0000-0001-7384-4851

Luis M. Gandía: 0000-0002-3954-4609

**Funding Sources**

Spanish Ministerio de Ciencia, Innovación y Universidades, and the European Regional Development Fund (ERDF/FEDER) (grant RTI2018-096294-B-C31 and grant PID2019-106687RJ-I00 /AEI/10.13039/501100011033). Gobierno de Navarra (project FOREST+, reference PC003-004). Obra Social "la Caixa" and Fundación Bancaria Caja Navarra.

**Notes**

The authors declare no competing financial interests.

## ACKNOWLEDGMENTS

Financial support from Gobierno de Navarra (grant PC003-004), Spanish Ministerio de Ciencia, Innovación y Universidades, the European Regional Development Fund (ERDF/FEDER) (grant RTI2018-096294-B-C31) and Agencia Estatal de Investigación (grant PID2019-106687RJ-I00 /AEI/10.13039/501100011033) is gratefully acknowledged. I. P. thanks Obra Social la Caixa, Fundación Caja Navarra and UPNA for their research contracts in the framework of the program “Captación del Talento 2019”. L. M. G. wishes to thank Banco de Santander and Universidad Pública de Navarra for their financial support under the “Programa de Intensificación de la Investigación 2018” initiative. Furthermore, the authors acknowledge Dr. Sara Marcelino for technical support with the SLA printing, the LMA-INA (Laboratorio de Microscopias Avanzadas – Instituto de Nanociencia de Aragon) for offering access to its

instruments and expertise, and the use of the Servicio de Difracción de Rayos X y Análisis por Fluorescencia del Servicio General de Apoyo a la Investigación-SAI at the Universidad de Zaragoza.

## ABBREVIATIONS

4NP: 4-Nitrophenol.

4AP: 4-Aminophenol.

ABS: Acrylonitrile Butadiene Styrene.

FFF: Fused Filament Fabrication.

FSP: Flame Spray Pyrolysis.

MB: Methylene Blue.

PDMS: Polydimethylsiloxane.

SLA: Stereolithography 3D printing

## REFERENCES

(1) Santana, H. S.; Silva, J. L.; Taranto, O. P. Development of Microreactors Applied on Biodiesel Synthesis: From Experimental Investigation to Numerical Approaches. *J. Ind. Eng. Chem.* **2019**, *69*, 1–12.

(2) Su, Y. H.; Song, Y.; Xiang, L. Continuous-Flow Microreactors for Polymer Synthesis: Engineering Principles and Applications. *Top. Curr. Chem.* **2018**, *376*, 44.

(3) He, Y.; Guo, S. H.; Chen, K. H.; Li, S. W.; Zhang, L. B.; Yin, S. H. Sustainable Green Production: A Review of Recent Development on Rare Earths Extraction and Separation Using Microreactors. *ACS Sustain. Chem. Eng.* **2019**, *7*, 17616–17626.

(4) Zhang, X. L.; Wiles, C.; Painter, S. L.; Watts, P.; Haswell, S. J. Microreactors as Tools for Chemical Research. *Chim. Oggi-Chem. Today* **2006**, *24*, 43–45.

(5) Suryawanshi, P. L.; Gumfekar, S. P.; Bhanvase, B. A.; Sonawane, S. H.; Pimplapure, M. S. A review on microreactors: Reactor Fabrication, Design, and Cutting-edge Applications. *Chem. Eng. Sci.* **2018**, *189*, 431–448.

(6) Rehm, T. H. Reactor Technology Concepts for Flow Photochemistry. *ChemPhotoChem* **2020**, *4*, 235-254.

(7) Shinozawa, Y.; Heggo, D.; Ookawara, S.; Yoshikawa, S. Photo-Fenton Degradation of Carbofuran in Helical Tube Microreactor and Kinetic Modeling. *Ind. Eng. Chem. Res.* **2020**, *59*, 3811–3819.

(8) Russo, V.; Protasova, L.; Turco, R.; de Croon, M.; Hessel, V.; Santacesaria, E. Hydrogen Peroxide Decomposition on Manganese Oxide Supported Catalyst: From Batch Reactor to Continuous Microreactor. *Ind. Eng. Chem. Res.* **2013**, *52*, 7668–7676.

(9) Xu, W. H.; Su, Y. H.; Song, Y.; Shang, M. J.; Zha, L.; Lu, Q. H. Process Analysis on Preparation of Cyclobutanetetracarboxylic Dianhydride in a Photomicroreactor within Gas-Liquid Taylor Flow. *Ind. Eng. Chem. Res.* **2018**, *57*, 2476–2485.

(10) Luo, X.; Su, P.; Zhang, W.; Raston, C. L. Microfluidic Devices in Fabricating Nano or Micromaterials for Biomedical Applications. *Adv. Mater. Technol.* **2019**, *4*, 1900488.

(11) Leblebici, M. E.; Stefanidis, G. D.; Van Gerven, T. Comparison of Photocatalytic Space-Time Yields of 12 Reactor Designs for Wastewater Treatment. *Chem. Eng. Process.* **2015**, *97*, 106–111.

(12) He, X. F.; Chen, R.; Zhu, X.; Liao, Q.; An, L.; Cheng, X.; Li, L. Optofluidics-Based Membrane Microreactor for Wastewater Treatment by Photocatalytic Ozonation. *Ind. Eng. Chem. Res.* **2016**, *55*, 8627–8635.

(13) Whitesides, G. M. The Origins and the Future of Microfluidics. *Nature* **2006**, *442*, 368–373.

(14) Tsao, C. W. Polymer Microfluidics: Simple, Low-Cost Fabrication Process Bridging Academic Lab Research to Commercialized Production. *Micromachines* **2016**, *7*, 225.

(15) McDonald, J. C.; Whitesides, G. M. Poly(dimethylsiloxane) as a Material for Fabricating Microfluidic Devices. *Acc. Chem. Res.* **2002**, *35*, 491–499.

(16) Duffy, D. C.; McDonald, J. C.; Schueller, O. J. A.; Whitesides, G. M. Rapid Prototyping of Microfluidic Systems in Poly(dimethylsiloxane). *Anal. Chem.* **1998**, *70*, 4974–4984.

(17) Kitson, P. J.; Glatzel, S.; Chen, W.; Lin, C. G.; Song, Y. F.; Cronin, L. 3D Printing of Versatile Reactionware for Chemical Synthesis. *Nat. Protoc.* **2016**, *11*, 920–936.

(18) Dragone, V.; Sans, V.; Rosnes, M. H.; Kitson, P. J.; Cronin, L. 3D-Printed Devices for Continuous-Flow Organic Chemistry. *Beilstein J. Org. Chem.* **2013**, *9*, 951–959.

(19) Parra-Cabrera, C.; Achille, C.; Kuhn, S.; Ameloot, R. 3D Printing in Chemical Engineering and Catalytic Technology: structured catalysts, mixers and reactors. *Chem. Soc. Rev.* **2018**, *47*, 209–230.

(20) Morgan, A. J. L.; Hidalgo San Jose, L.; Jamieson, W. D.; Wymant, J. M.; Song, B.; Stephens, P.; Barrow, D. A.; Castell, O. K. Simple and Versatile 3D Printed Microfluidics Using Fused Filament Fabrication. *PLoS One* **2016**, *11*, e0152023.

(21) Tothill, A. M.; Partridge, M.; James, S. W.; Tatam, R. P. Fabrication and Optimisation of a Fused Filament 3D-Printed Microfluidic Platform. *J. Micromech. Microeng.* **2017**, *27*, 035018.

(22) Zein, I.; Hutmacher, D. W.; Tan, K. C.; Teoh, S. H. Fused Deposition Modeling of Novel Scaffold Architectures for Tissue Engineering Applications. *Biomaterials* **2002**, *23*, 1169–1185.

(23) Ning, F.; Cong, W.; Qiu, J.; Wei, J.; Wang, S. Additive Manufacturing of Carbon Fiber Reinforced Thermoplastic Composites Using Fused Deposition Modeling. *Compos. Pt. B-Eng.* **2015**, *80*, 369–378.

(24) Castedo, A.; Mendoza, E.; Angurell, I.; Llorca, J. Silicone Microreactors for the Photocatalytic Generation of Hydrogen. *Catal. Today* **2016**, *273*, 106–111.

(25) Comina, G.; Suska, A.; Filippini, D. PDMS Lab-on-a-Chip Fabrication Using 3D printed Templates. *Lab Chip* **2014**, *14*, 424–430.

(26) Castedo, A.; Uriz, I.; Soler, L.; Gandía, L. M.; Llorca, J. Kinetic Analysis and CFD Simulations of the Photocatalytic Production of Hydrogen in Silicone Microreactors from Water-Ethanol mixtures. *Appl. Catal. B–Environ.* **2017**, *203*, 210–217.

(27) Castedo, A.; Casanovas, A.; Angurell, I.; Soler, L.; Llorca, J. Effect of Temperature on The Gas-Phase Photocatalytic $H_2$ Generation Using Microreactors under UVA and Sunlight Irradiation. *Fuel* **2018**, *222*, 327–333.

(28) Saggiomo, V.; Velders, A. H. Simple 3D Printed Scaffold-Removal Method for the Fabrication of Intricate Microfluidic Devices. *Adv. Sci.* **2015**, *2*, 1500125.

(29) Yamashita, T.; Yasukawa, K.; Yunoki, E. Fabrication of a Polydimethylsiloxane Fluidic Chip Using a Sacrificial Template Made by Fused Deposition Modeling 3D Printing and Application for Flow-injection Analysis. *Anal. Sci.* **2019**, *35*, 769–775.

(30) Pellejero, I.; Clemente, A.; Reinoso, S.; Cornejo, A.; Navajas, A.; Vesperinas, J. J.; Urbiztondo, M. A.; Gandía, L. M. Innovative Catalyst Integration on Transparent Silicone Microreactors for Photocatalytic Applications. *Catal. Today* **2020**, *https://doi.org/10.1016/j.cattod.2020.05.058*.

(31) Kotz, F.; Risch, P.; Helmer, D.; Rapp, B. E. High-Performance Materials for 3D Printing in Chemical Synthesis Applications. *Adv. Mater.* **2019**, *31*, 1805982.

(32) Skorski, M. R.; Esenther, J. M.; Ahmed, Z.; Miller, A. E.; Hartings, M. R. The Chemical, Mechanical, and Physical Properties of 3D Printed Materials Composed of $TiO_2$-ABS Nanocomposites. *Sci. Technol. Adv. Mater.* **2016**, *17*, 89–97.

(33) Bible, M.; Sefa, M.; Fedchak, J. A.; Scherschligt, J.; Natarajan, B.; Ahmed, Z.; Hartings, M. R. 3D-Printed Acrylonitrile Butadiene Styrene-Metal Organic Framework Composite Materials and Their Gas Storage Properties. *3D Print. Addit. Manuf.* **2018**, *5*, 63–72.

(34) Aumnate, C.; Pongwisuthiruchte, A.; Pattananuwat, P.; Potiyaraj, P. Fabrication of ABS/Graphene Oxide Composite Filament for Fused Filament Fabrication (FFF) 3D Printing. *Adv. Mater. Sci. Eng.* **2018**, *2018*, 2830437.

(35) Mueller, R.; Mädler, L.; Pratsinis, S. E. Nanoparticle Synthesis at High Production Rates by Flame Spray Pyrolysis. *Chem. Eng. Sci.* **2003**, *58*, 1969–1976.

(36) Strobel, R.; Baiker, A.; Pratsinis, S. E. Aerosol Flame Synthesis of Catalysts. *Adv. Powder Technol.* **2006**, *17*, 457–480.

(37) REHAU Acrylonitrile-Butadiene-Styrene (RAU-ABS) Material Data Sheet AV0270 EN. **2013**.

(38) Shahinyan, G. A.; Amirbekyan, A. Y.; Markarian, S. A. Photophysical Properties of Methylene Blue in Water and in Aqueous Solutions of Dimethylsulfoxide. *Spectrochim. Acta A* **2019**, *217*, 170–175.

(39) Zhang, L.; Liu, Z.; Wang, Y.; Xie, R.; Ju, X.-J.; Wang, W.; Lin, L.-G.; Chu, L.-Y. Facile Immobilization of Ag Nanoparticles on Microchannel Walls in Microreactors for Catalytic Applications. *Chem. Eng. J.* **2017**, *309*, 691–699.

(40) Height, M. J.; Pratsinis, S. E.; Mekasuwandumrong, O.; Praserthdam, P. Ag-ZnO Catalysts for UV-Photodegradation of Methylene Blue. *Appl. Catal. B-Environ.* **2006**, *63*, 305–312.

(41) Bernareggi, M.; Dozzi, M. V.; Bettini, L. G.; Ferretti, A. M.; Chiarello, G. L.; Selli, E. Flame-Made Cu/$TiO_2$ and Cu-Pt/$TiO_2$ Photocatalysts for Hydrogen Production. *Catalysts* **2017**, *7*, 301.

(42) Akurati, K. K.; Vital, A.; Dellemann, J.-P.; Michalow, K.; Graule, T.; Ferri, D.; Baiker, A. Flame-Made $WO_3$/$TiO_2$ Nanoparticles: Relation Between Surface Acidity, Structure and Photocatalytic Activity. *Appl. Catal. B-Environ.* **2008**, *79*, 53–62.

(43) Spurr, R. A.; Myers, H. Quantitative Analysis of Anatase-Rutile Mixtures with an X-Ray Diffractometer. *Anal. Chem.* **1957**, *29*, 760–762.

(44) Choudhury, B.; Dey, M.; Choudhury, A. Defect Generation, d-d Transition, and Band Gap Reduction in Cu-doped $TiO_2$ Nanoparticles. *Int. Nano Lett.* **2013**, *3*, 25.

(45) Zhen, W.; Jiao, W.; Wu, Y.; Jing, H.; Lu, G. The Role of a Metallic Copper Interlayer During Visible PhotocatalyticHydrogen Generation over a $Cu/Cu_2O/Cu/TiO_2$ Catalyst. *Catal. Sci. Technol.* **2017**, *7*, 5028–5037.

(46) Zhao, Y.; Chen, J.; Cai, W.; Bu, Y.; Huang, Q.; Tao, T.; Lu, J. CuO-Decorated Dual-Phase $TiO_2$ Microspheres with Enhanced Activity for Photocatalytic $CO_2$ Reduction in Liquid–Solid Regime. *Chem. Phys. Lett.* **2019**, *725*, 66–74.

(47) Saran, S.; Manjari, G.; Devipriya, S. P. Synergistic Eminently Active Catalytic and Recyclable Ag, Cu and Ag-Cu Alloy Nanoparticles Supported on $TiO_2$ for Sustainable and Cleaner Environmental Applications: A Phytogenic Mediated Synthesis. *J. Clean. Prod.* **2018**, *177*, 134–143.

(48) Sangpour, P.; Hashemi, F.; Moshfegh, A. Z. Photoenhanced Degradation of Methylene Blue on Cosputtered M:$TiO_2$ (M = Au, Ag, Cu) Nanocomposite Systems: A Comparative Study. *J. Phys. Chem. C* **2010**, *114*, 13955–13961.

(49) Rather, R. A.; Singh, S.; Pal, B. Photocatalytic Degradation of Methylene Blue by Plasmonic Metal-$TiO_2$ Nanocatalysts under Visible Light Irradiation. *J. Nanosci. Nanotechnol.* **2017**, *17*, 1210-1216.

(50) Gao, F.; Jiang, J.; Du, L. Y.; Liu, X. F.; Ding, Y. Q. Stable and Highly Efficient $Cu/TiO_2$ Nanocomposite Photocatalyst Prepared Through Atomic Layer Deposition. *Appl. Catal. A-Gen.* **2018**, *568*, 168–175.

(51) Chausse, V.; Llorca, J. Photoproduction of Hydrogen in Microreactors: Catalytic Coating or Slurry Configuration? *Catal. Today* **2020***, https://doi.org/10.1016/j.cattod.2020.08.021*

**SYNOPSIS.** Fused filament 3D printing was used for easy, fast and cheap fabrication of microreactor for photocatalytic applications.

**TOC**